Engineered Science

REVIEW PAPER View Article Online

# Electrodes with High Conductivities for High Performance Lithium/Sodium Ion Batteries

Litao Yan,† Haizhen Wang,† Di Huang and Hongmei Luo*

Electrochemical devices including lithium/sodium-ion batteries and supercapacitors, as the promising solution to energy storage and environmental issues in the future, have attracted great attention recently due to the rapidly growing demand for non-renewable resources. The common electrode materials, including metal oxides, suffer from low conductivities, which lead to low charge transfer rate during the charge/discharge process and thus poor battery performance such as low specific capacitance/capacity, low rate capability, and poor cycling stability. Therefore, researchers have been searching for various strategies to enhance the conductivity of the electrode materials and thus the performance of lithium/sodium-ion batteries and supercapacitors. In this mini-review, different strategies to enhance the conductivities of the electrode materials would be discussed which will provide researchers various routes to improve the conductivity of the electrode materials in order to improve the performance of electrochemical device.

**Keywords:** lithium/sodium batteries, supercapacitors, conductivity, electrode materials, electrochemical devices

**Received 6th March 2018, Accepted 18th March 2018**

**DOI: 10.30919/es.180318**

## 1. Introduction

The combustion of fossil fuel leads to the emission of global warming gas including carbon dioxide and other gases, resulting in various environmental issues. The utilization of renewable energy resources including solar, wind and hydropower energy can not only effectively reduce the greenhouse gas emission but also decrease the rapidly growing demand for non-renewable resources.[1–3] The critical energy storage issue for the utilization of renewable energy resource during the on-peak period limits the extensive applications of renewable technologies.[4,5] Electrochemical devices including batteries and supercapacitors, as the promising solution to energy storage and environmental issues in the future, have attracted great attention since they could average out the production of renewable resources and fill the gap of energy shortage during the on-peak period.[5–7]

Batteries and supercapacitors, the typical electrochemical energy storage devices, consist of two electrodes and ion conducting

*Department of Chemical and Materials Engineering, New Mexico State University, New Mexico 88003, United States. E-mail: hluo@nmsu.edu*
† Those authors contribute equally.

**Litao Yan**

*Litao Yan is currently a postdoctoral at Pacific Northwest National lab. He got Ph.D degree in chemical Engineering at New Mexico State University. His research interest lies in lithium ion batteries, fuel cells and flow batteries. He received his B. S. degree in Materials Physics from Lanzhou University in 2007 and M.S. in Materials Science from the University of Science and Technology of China in 2010.*

**Haizhen Wang**

*Haizhen Wang is a Ph.D. student in Department of Chemical and Materials Engineering at New Mexico State University. She received her B.S. degree in Chemistry from Liaocheng University and M.S. degree in Inorganic chemistry from University of Science and Technology of China (USTC). Her research interest mainly focuses on the design of transition metal-based bifunctional electrocatalysts as well as anode materials for lithium ion batteries.*

electrolyte.[8] The charge/discharge process associated with ions intercalation-de-intercalation between two electrodes can realize the energy storage and release process. The electrochemical properties of two electrodes could determine the performance of batteries and supercapacitors. Therefore, it is expected that the energy and power density of batteries could be increased by the optimization of the electrode materials. Up to now, graphite, lithium titanate ($Li_4Ti_5O_{12}$), silicon, transition metal oxides and metal sulfides have been employed as anode materials for batteries and supercapacitors.[9–21] However, among all the anode materials, only the conductivity of commercial graphite and porous carbon can meet the requirements as electrodes for lithium ion batteries (LIBs) and supercapacitors, respectively. The poor electronic conductivities of lithium titanate, silicon, transition metal oxides and metal sulfides will reduce the charge transfer during the discharge/charge processes for supercapacitors and batteries, which limits their further performance improvement.[10,22–26]

To enhance the electrode conductivities in those electrochemical devices in order to optimize their electrochemical performance, ongoing research focuses on improving the charge transfer and ion diffusion by incorporation of conductive materials into electrodes including graphene based materials,[27,28] high surface area mesoporous carbon,[13,29] and carbon nanotubes;[30] and introduction of conductive layer on active materials such as carbon coating;[31,32] reducing the size of the electrode materials to nanoscale.[5] With the unique structural, mechanical and electrical properties of the critical conductive materials, the composite electrodes can enhance the electron transport, realize fast charge transfer and ion diffusion, resulting in improved capacity and cyclability and consequently high electrochemical performance, since the conductive materials could function as buffering components and serve as the backbone in the electrode materials to prevent the detachment and agglomeration of metal oxides. Therefore, it is of great importance to familiarize researchers with different approaches to improve the conductivities of the electrode materials. This review will not cover all the information of LIBs with high conductive electrode materials. Instead, the recent developments of different strategies to create highly conductive composite electrode materials in LIBs especially in our group will be summarized. It is expected that this mini review will be of great benefit to scientists and researchers who are interested in the high-performance LIBs with highly conductive electrode materials.

## 2. Electrochemical energy storage devices

Batteries and supercapacitors (SCs), two typical electrochemical energy storage devices, have been regarded as the dominant power sources for our personal electronics and electrical vehicles.[4,33,34] A typical battery or supercapacitor system consists of a negative electrode (anode, e.g., graphite for LIBs, hard carbon for sodium ion batteries (SIBs) or active carbon for SCs), an ion conducting electrolyte, and a positive electrode (cathode, e.g., $LiMn_{1/3}Co_{1/3}Ni_{1/3}O_2$ and $LiCoO_2$ for LIBs or active carbon for SCs),[5] as shown in Fig. 1. The working principle of batteries and SCs involves the cations ($Li^+$, $Na^+$, and $H^+$) and anions ($OH^-$) diffusion from one electrode to the other under the voltage-driven force and the redox reactions will take place at two electrodes. Moreover, electrons will flow toward the external circuit in order to maintain the system charge neutrality. Although LIBs with graphite as anodes are commercially available, the low theoretical capacity of graphite still limits its application in the next-generation high performance LIBs. Besides, the most promising electrodes including metal oxides suffer from low electrical conductivities which also limit their commercialization. Therefore, it is valuable to develop electrodes with high conductivities in order to realize high performance LIBs. Except for LIBs, SIBs (Fig. 1c) have also been investigated extensively due to rich sodium resources with low cost. However, the sluggish kinetics of sodium ions, resulted from large radius of sodium ion (compared with lithium ions), lead to low energy density and poor electrochemical performance of the batteries.[15,24,35] Therefore, electrode materials with high conductivities will also be necessary for SIBs to achieve high energy/power density and cycle stability. Meanwhile, the hybrid supercapacitors (Fig. 1b) with metal oxides (pseudocapactive behavior) as positive electrodes can be an efficient way to

**Di Huang**

*Di Huang is a Ph.D. student in Department of Chemical and Materials Engineering at New Mexico State University with a research interest in the development of novel cathode materials for lithium ion batteries. He received his B.S. degree in Chemical Engineering from East China University of Science and Technology in 2013 and M.S. degree in Chemical Engineering at New Mexico State University in 2015.*

**Hongmei Luo**

*Hongmei Luo is currently a Luke Barry Shires Endowed Associate Professor in Chemical Engineering at New Mexico State University. She received her B.S. (1992) in chemistry from Fuyang Normal University, China, and Ph.D. (2006) in chemical engineering from Tulane University. She was a postdoctoral research associate at Los Alamos National Laboratory from 2006 to 2009 and she joined NMSU in fall, 2009. Her group research focuses on epitaxzial oxide thin films and nanostructured materials for magnetic, optoelectronics, catalysis, and renewable energy applications.*

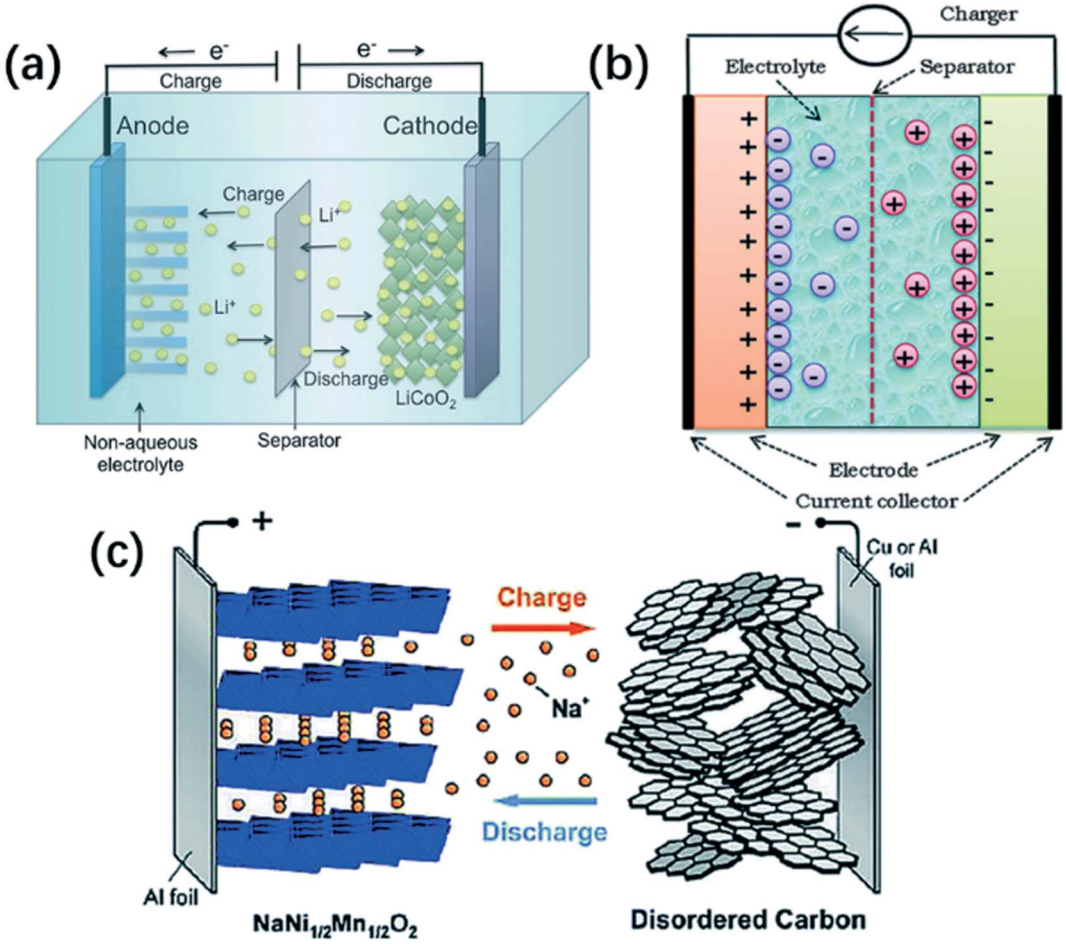


**Fig. 1** Schematic illustration of (a) a lithium ion battery; (b) an electrochemical supercapacitor and (c) sodium ion battery. Adapted and reproduced with the permission from Ref. 39. Copyright 2015; Ref. 40. Copyright 2015; Ref. 41. Copyright 2012, Royal Society of Chemistry.

increase the energy density of SCs.[36,37] Similar to LIBs or SIBs with metal oxides as electrodes, the low conductivities of most metal oxides lead to low rate performance and low power densities in SCs as well. Only hybrid supercapacitor with high conductive noble metal oxide $RuO_2$ as electrode has delivered superior specific capacitance and cycling stability. However, the high cost of $RuO_2$ motivates us to seek for alternative cheaper metal oxides as electrodes in hybrid supercapacitors.[38] As discussed above, metal oxides with high theoretical capacity generally suffer from the low conductivities. Thus, developing electrodes with high conductivities plays a vital role in achieving the high performance electrochemical energy storage devices including both batteries and supercapacitors.

# 3. Strategies to improve electrode conductivities

## 3.1. Graphene or reduced graphene oxide (rGO)-based composites

Graphene and reduced graphene oxide (rGO) have been good candidates for constructing graphene-based composite materials with metal oxides to enhance the conductivities of the electrodes due to their specific open porous two-dimensional structure, large surface area and excellent electronic conductivity.[3,14,42–46] The conductivity of electrode materials could be significantly improved after combining with graphene or rGO.[26,47–49] In addition, the high surface area of graphene or rGO can balance the volume change stress during charge and discharge processes, especially for high capacity and high rate electrode materials.[47,50–52] It has been widely reported that incorporation of graphene or rGO with active electrode materials (e.g. metal oxides, metal sulfides and silicon) results in excellent battery performance compared to the corresponding pure active electrode materials.[3,28,47,53] The functional groups with negative charge on the surface of rGO nanosheets provide the platform that the transition metal ions with positive charge can be easily absorbed by and uniformly distributed onto the GO nanosheets. The stabilized metal ions on GO nanosheets can interact with those negative functional groups to form active electrode materials/GO nanosheets composites. Highly conductive rGO could be obtained after the post heat treatment of GO under reduction atmosphere. Recently, a new nanocomposite formulation of the FeS-based anode for LIBs has been proposed, where FeS nanoparticles embedded in rGO have been produced via a facile direct-precipitation approach[14] and employed as high performance electrode materials for LIBs. During synthesis process, the functional groups (e.g., −OH, −COOH) with negative charges on the surface of GO have strong columbic interaction with the $Fe^{3+}$ ions and the introduction of $Na_2S$ leads to the

 

formation of the FeS precipitate. Finally, small FeS nanoparticles are wrapped by rGO nanosheets, which can increase their electronic conductivity and prevent the polysulfide dissolution, resulting in the enhanced electrochemical performance.

In addition, graphene with high surface area and high electronic conductivity would also enhance the charge transfer and ion diffusion, resulting in high performance batteries and supercapacitors.[51,54–58] For example, $Nb_2O_5$/graphene paper electrode could be prepared by hydrothermal reaction of niobium precursor and graphene,[57] as shown in Fig. 2. The ion diffusion could be enhanced due to the channels between two compact layers, as can be seen from the SEM images (Fig. 2 a-f). TEM images (Fig. 2 g-i) clearly showed that ultrafine $Nb_2O_5$ nanoparticles (average size of 1-3 nm) were uniformly distributed on the graphene nanosheets.

$TiO_2$/graphene also has been studied as promising anode materials for lithium ion batteries with fairly good performance.[27,59] For example, self-assembled $TiO_2$/graphene showed enhanced lithium ion insertion/extraction kinetics in $TiO_2$, and thus delivered high charge/discharge rate performance.[27] Besides, rGO–$TiO_2$ nanospheres as electrodes for sodium ion battery demonstrated a capacity of 300 mA h $g^{-1}$ and excellent cycling stability with a capacity retention of 208 mA h $g^{-1}$ over 300 cycles,[35] which further confirmed that uniform conductive network coating on metal oxide can efficiently increase the conductivities of metal oxide electrode materials and thus the electrochemical performance of the batteries.

Ultrafine $TiO_2$ and $Nb_2O_5$ nanocrystals uniformly anchored on reduced graphene oxide by controllable hydrolysis of titanium and niobium precursors, respectively, have been investigated as promising anode materials for high performance lithium ion batteries and sodium ion batteries by our group. The interactions between the functional groups (e.g. $OH^-$, and $COO^-$ with negative charge on the surface of GO) and niobium or titanium precursor (positive charge) lead to the amorphous niobium/titanium hydroxide thin layer uniformly anchoring on the surface of GO sheets at step 1. During step 1, introducing proper amount of water can result in the controllable hydrolysis of the precursors which can prevent the aggregation of amorphous niobium/titanium hydroxide nanoparticles and result in metal hydroxides uniformly coating on GO nanosheet. After annealing at 450 °C under forming gas, amorphous hydroxide layers would convert to $TiO_2$ or $Nb_2O_5$ nanocrystals with particle size of around 5 nm or 3 nm, respectively, and GO reduced to rGO simultaneously with enhanced conductivity. The architecture of ultrafine $TiO_2$[60] or $Nb_2O_5$[61] nanocrystals anchored on highly conductive rGO network can not only enhance charge transfer and buffer the volume change during lithiation/delithiation or sodiation/desodiation processes, but also provide more active surface area for lithium or sodium ion storage, resulting in superior rate and cycle performance.

Fig. 3a displays the typical TEM image of ultrafine $Nb_2O_5$ NCs and the nanocrystals stayed on the surface of rGO. The rate capability of $Nb_2O_5$ NCs/rGO could achieve as high as 85 mA h $g^{-1}$ at a

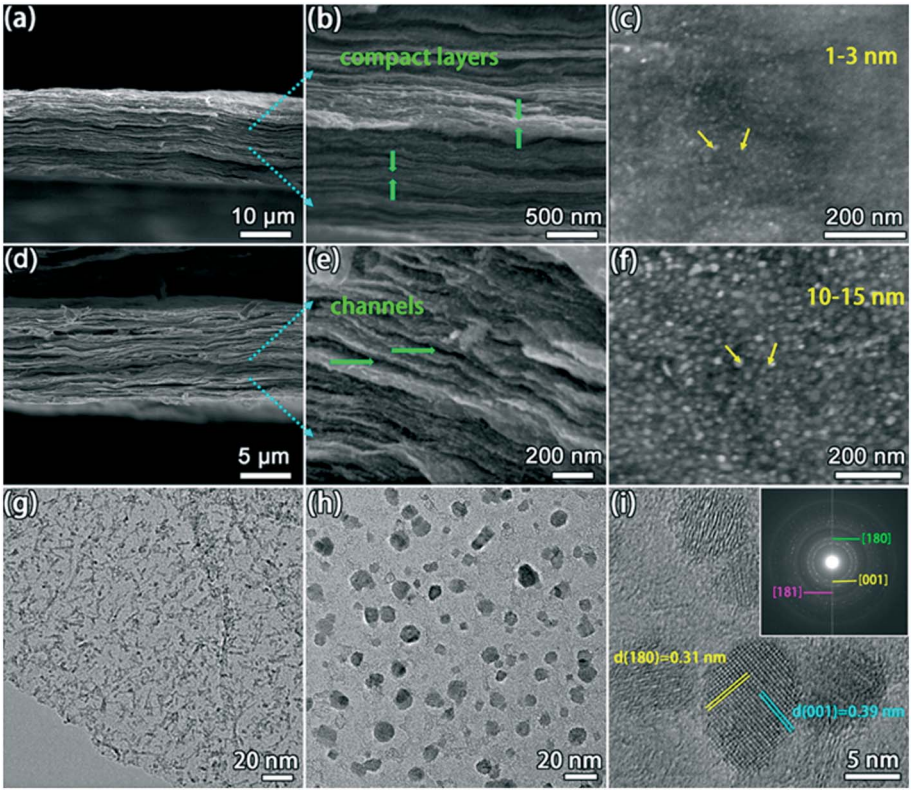


**Fig. 2** SEM images of $Nb_2O_5$/rGO (a-c); T-$Nb_2O_5$/graphene composite papers (d-f); TEM image of $Nb_2O_5$/rGO (g-h); HRTEM and electron diffraction pattern (i) of T-$Nb_2O_5$/graphene. Adapted and reproduced with the permission from Ref. 57. Copyright 2015, American Chemical Society.

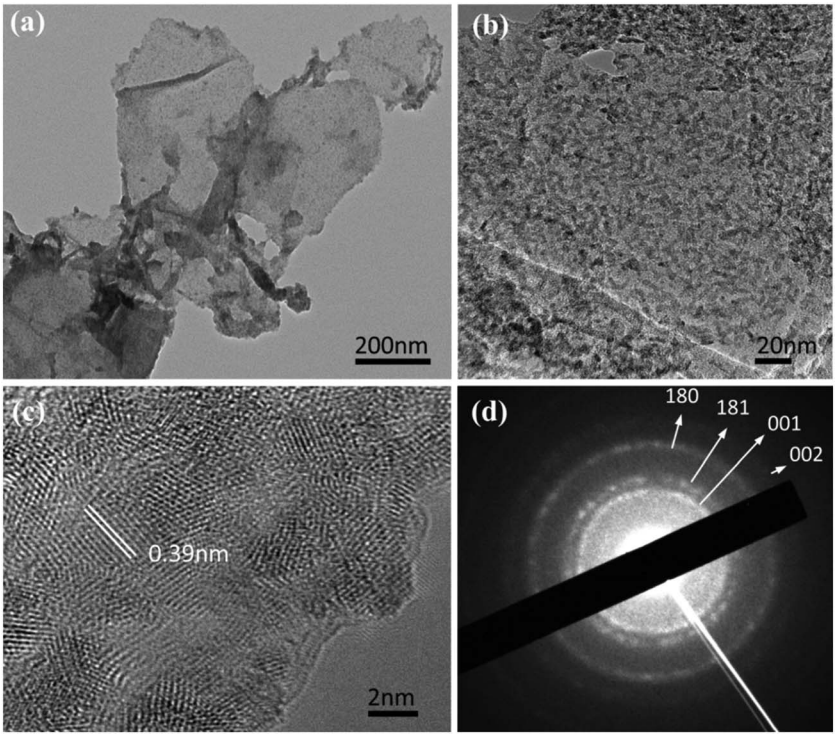


**Fig. 3** (a) The TEM image of niobium hydroxide and graphene oxide after coating process; (b, c) HRTEM images of $Nb_2O_5$ NCs/rGO; and (d) SAED pattern of $Nb_2O_5$ NCs/rGO. Adapted and reproduced with the permission from Ref. 61. Copyright 2016, American Chemical Society.

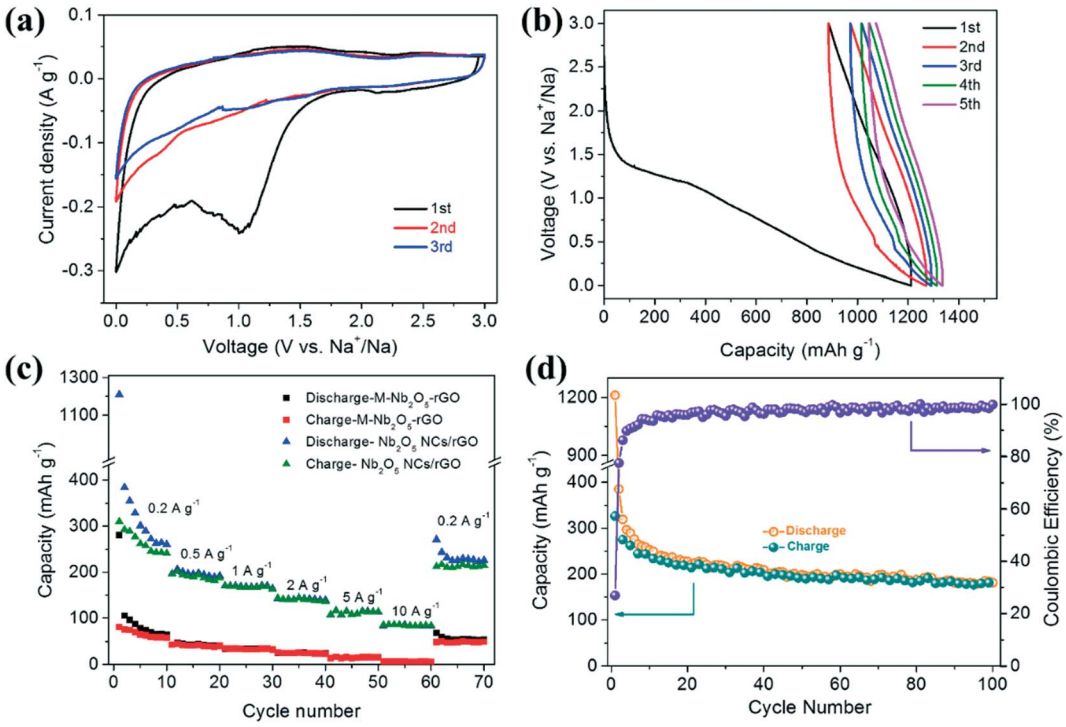


**Fig. 4** (a) CV curves of $Nb_2O_5$ NCs/rGO at a scan rate of 0.1 mV $s^{-1}$; (b) galvanostatic discharge/charge profiles of $Nb_2O_5$ NCs/rGO at 0.2 A $g^{-1}$; (c) rate capability of $Nb_2O_5$ NCs/rGO and the mixture of $Nb_2O_5$ and rGO at various current densities from 0.2 to 10 A $g^{-1}$; and (d) cycling performance and corresponding Coulombic efficiency of $Nb_2O_5$ NCs/rGO at 0.2 A $g^{-1}$ (voltage range: 0-3 V). Adapted and reproduced with the permission from Ref. 61. Copyright 2016, American Chemical Society.

 

current density of 10 A h $g^{-1}$ while almost no capacity could be observed for mixture of $Nb_2O_5$ and rGO, as shown in Fig. 4c. The poor performance of the mixture can be ascribed to the large particle size and non-robust combination of $Nb_2O_5$ in the M-$Nb_2O_5$-rGO (Fig. 5a). It is noted that the covalent bonding between GO and niobium precursor can produce uniform coating on GO, so that ultrafine $Nb_2O_5$ on rGO could be obtained after heat treatment under the forming gas. However, larger particle size of $Nb_2O_5$ was obtained when no GO was added into the solution during the hydrolysis process.

The cycle durability at a current density of 0.2 A $g^{-1}$ for NCs/rGO also has been examined (Fig. 4c). The first discharge capacity delivered around 1200 mAh $g^{-1}$, and then stable reversible capacity as high as 242 mAh $g^{-1}$ could be achieved after 30 cycles. The Coulombic efficiency (CE) is nearly 100 %. The reversible capacity could maintain around 60 mAh $g^{-1}$ after 5000 cycles (Fig. 5b), indicating fairly long-term cycling stability. The high rate performance and long-term cycling performance could be ascribed to the ultrafine $Nb_2O_5$ and high conductive rGO network in which the ultrafine $Nb_2O_5$ NCs provide more active surface area and the high conductive rGO can enhance the charge transfer. Metal oxide nanoparticles anchored on the surface of rGO platelets act as spacers between these platelets and rGO not only acts as a conductive additive but also offers sites for lithium insertion/desertion during charge and discharge process thus improve the battery performance. However, for the M-$Nb_2O_5$-rGO, the capacity decreased to 30 mAh $g^{-1}$ after 100 cycles, as shown in Fig. 5c. These examples have further confirmed the feasibility of using both graphene and rGO to enhance the electrode conductivities of electrochemical devices.

In addition to graphene and rGO, graphite also has been proposed to be a good candidate to improve the conductivity of electrode materials. Fei et al developed[62] a $Co_3O_4$/graphite composite material, in which the graphite as an additive material, significantly enhanced the battery performance compared to pristine $Co_3O_4$ due to its high conductivity and structural stability. The $Co_3O_4$ was synthesized by hydrothermal method shown as follows:

$$Co^{2+} + 6NH_3 \leftrightarrow \left[Co(NH_3)_6\right]^{2+} \quad (1)$$

$$\left[Co(NH_3)_6\right]^{2+} + 2OH^- \rightarrow Co(OH)_2 + 6NH_3 \quad (2)$$

$$6Co(OH)_2 + O_2 \rightarrow 2Co_3O_4 + 6H_2O \quad (3)$$

In order to study the effect of graphite, three groups of samples have been prepared. Group A is the pristine $Co_3O_4$. In group B, 0.1g graphite was added before the hydrothermal step and removed after post annealing step. And in group C, the same amount of graphite was added and retained after post annealing step. XRD patterns proved $Co_3O_4$ with cubic structure has been successfully synthesized. No impurity phases were detected in group A and B. However, in group C, two extra peaks which can be indexed as graphite were detected and 21 wt % of graphite in group C was then quantitatively measured and confirmed by TGA. TEM images revealed the remarkable morphology change from nanowire to nanoparticle due to the addition of graphite. Possible mechanism for morphology change has been proposed. It is noted that crystals are likely to grow along the same direction to form nanowires as a result of the hydrogen bonding reaction. Nevertheless, when graphite was introduced into hydrothermal reaction, hydroxyl group on graphite surface would attract the Co and further disorganize its morphology, thereby forming nanoparticles instead of nanowires. Eventually, the half-cell test stated that $Co_3O_4$/graphite with a capacity of 1082 mAh $g^{-1}$ at low current density of 100 mA $g^{-1}$ presents an excellent cyclic performance and rate capability, indicating that additional graphite extraordinarily improves the pure $Co_3O_4$ battery performance.

### 3.2. Carbon nanotubes-based composites

Carbon nanotubes (CNTs) with one-dimensional (1D) nanostructures and high electronic conductivities make them the promising conductive agents in the application of electrochemical energy storage devices since they take the advantage of directional electronic and ionic transportation, leading to high electronic and ion conductivities.[30,36,63–67] For the composites based on CNTs and transition metal oxides, CNTs are ideal conducting path to ensure a good charge propagation. Besides, they serve as a perfect skeleton with stretchable properties that significantly improves the cyclability

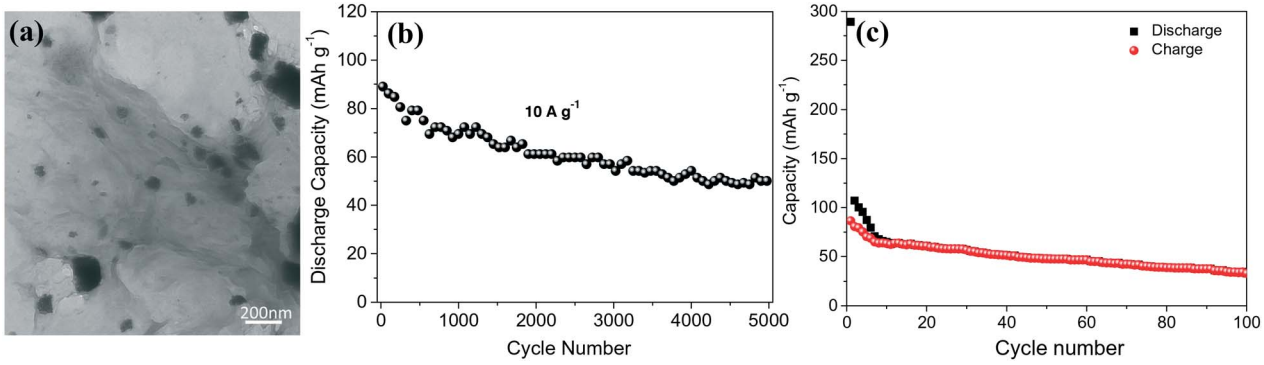


**Fig. 5** (a) TEM image of mechanically mixed $Nb_2O_5$ and rGO; (b) Cycle performance of $Nb_2O_5$ NCs/rGO at a current density of 10 A $g^{-1}$; (c) The cycling stability of the mechanically mixed $Nb_2O_5$ and rGO. Adapted and reproduced with the permission from Ref. 61. Copyright 2016, American Chemical Society.

of electrochemical devices through decreasing the volumetric changes of material during charging/discharging. Recently, highly porous $MnO_2$ nanoflakes/carbon nanotube (CNT) nanocomposites were employed as the promising anode materials for high performance LIBs, delivering a large reversible capacity of 801 mAh $g^{-1}$, high rate and high durability.[68] The excellent electrochemical performance of the $MnO_2$/CNT nanocomposite electrode can be attributed to its unique hierarchy architecture (Fig. 6a-b) and high conductivities of electrode after combining with CNTs, providing fast lithium ion and electron transport. Except for $MnO_2$/CNT composite, $Fe_3O_4$ sheath (particle size of 5−7 nm)/aligned carbon nanotube (CNT) scaffolds (Fig. 6c-d) composite electrode also showed a high reversible capacity of 800 mAh $g^{-1}$ and high rate capability.[69] The superior electrical conductivity of CNTs maintains the charge transfer of $Fe_3O_4$ sheath/CNT composite electrode during charge/discharge process. Hybridization of CNTs with $TiO_2$ and $LiNbO_3$ is considered to be the most facile and effective approach since CNTs can facilitate faster electron transfer and also provide more $Li^+$ diffusion paths, which would increase the performance of LIBs.[70,71]

Similar to the uniform $TiO_2$ coating on graphene, $TiO_2$ coating on CNTs also has been proposed and utilized as electrode in lithium ion batteries to increase the electrochemical performance. $TiO_2$, a promising material with high energy density and durability, has been widely used in supercapacitors or LIBs. Meanwhile CNTs as 3D material, not only function as a template to control the morphologies, but also strengthen the electrochemical performance of $TiO_2$ due to its high conductivity. Recently, we have developed a hybrid material consisting of uniform porous $TiO_2$ coating on CNTs prepared by sol-gel method. The porous $TiO_2$/CNTs hybrids were synthesized via hydrolysis reaction of titanium isopropoxide on the surface of CNTs. TEM images show that continuous porous $TiO_2$ was uniformly coated on CNTs with a thickness of ~20 nm. Anatase $TiO_2$ phase was confirmed by XRD pattern and Raman spectra indicate the existence of anatase $TiO_2$ and CNTs, respectively. High resolution TEM was also used to verify the porous structure with pore size $< 10$ nm. Moreover, to study the importance of the contact between $TiO_2$ and CNTs, a controlled group was established, in which the same mass ratio of non-functionalized CNTs were added. It has been reported that, compared with the mixture of $TiO_2$ and non-functionalized CNTs, the porous $TiO_2$/CNTs shows a comparable initial discharge/charge capacity (268 and 207 mAh $g^{-1}$, respectively), superior durability and stability. The retention of 97 % among the current density increased from 0.2 A $g^{-1}$ to 1.6 A $g^{-1}$ and decreased back to 0.2 A $g^{-1}$, suggesting that the strong interaction between $TiO_2$ and CNTs has a dominate impact on electrical performance. In conclude, it has been stated that the superior electrical performance of the porous $TiO_2$/CNTs can be attributed to following factors: 1) the porous structure boosts lithium ions diffusion by providing a shorter diffusion path; 2) CNTs as highly ordered-materials with good conductivity not only benefit the current collecting, but also form strong interaction with $TiO_2$ which plays a vital role in maintaining the stability of electrode during charge/discharge process.

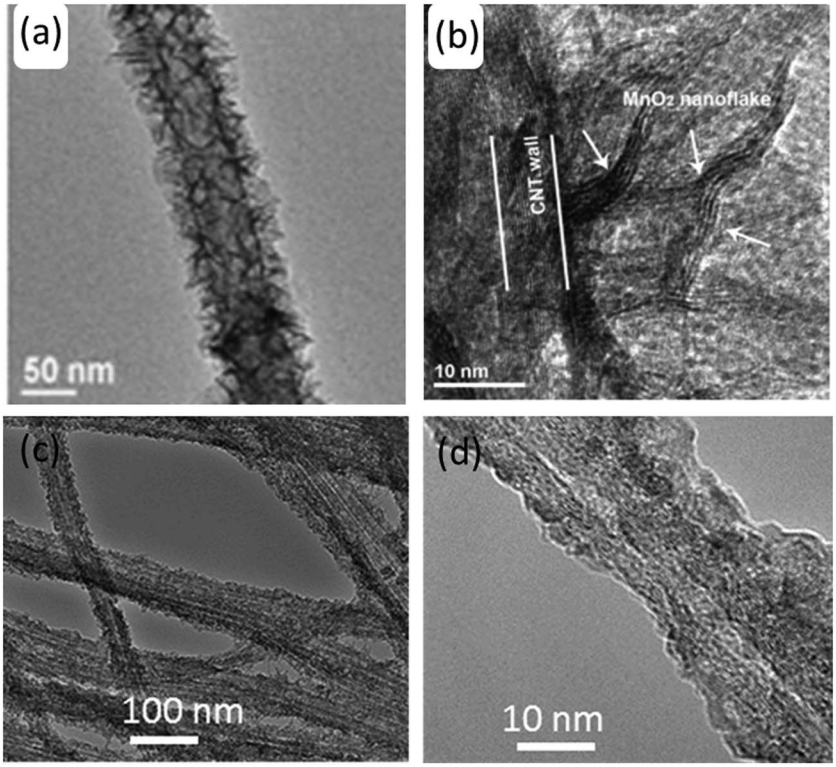


**Fig. 6** TEM images of $MnO_2$ nanoflakes/carbon nanotube (a-b), adapted and reproduced with the permission from Ref. 68 Copyright 2010, Royal Society of Chemistry; and $Fe_3O_4$ sheath/CNT (c-d), adapted and reproduced with the permission from Ref. 69. Copyright 2013, American Chemical Society.

 

### 3.3. 3D mesoporous carbon-based composites

Recently, the instant gelation method has been proposed to prepare 3D mesoporous $MoS_2$@C composite.[72] The jelly-like semisolid would form after combining silicon based macromolecules and other macromolecules such as sugar since they are rich in hydroxyl (-OH) groups and can bind with polyatomic anions such as $MoS_4^{2-}$. The subsequent calcination process can lead to the formation of $SiO_2$ network and 3D carbon network after the carbonization process of sugar. $SiO_2$ network could be removed using NaOH solution, resulting in final product with mesoporous structure and high surface area. Therefore, it can be used to prepare numerous 3D carbon composites with metal oxides, metal nitrides and metal sulfides. The LIBs with 3D $MoS_2$@C composite as anode materials delivered enhanced electrochemical performance compared with pure $MoS_2$. The conductive 3D carbon matrix not only promotes charge transfer but also prevents structural collapse of the electrode materials due to huge volume changes during the charging/discharging cycles. Moreover, numerous micropores and mesopores in the 3D carbon matrix can facilitate the ion diffusion to active sites with less resistance, resulting in enhanced charge transfer and thus better electrochemical performance. Recently, we have also successfully designed and prepared hierarchical $MoS_2$–C microspheres by a facile and scalable ultrasonic nebulization route.[73] The space between few-layer $MoS_2$ nanosheets is filled and bridged with mesoporous carbon, as shown in Fig. 7a-d. The hierarchical $MoS_2$–C microspheres exhibited excellent electrochemical properties including low resistance, high rate capacity (a capacity of 730 mAh $g^{-1}$ at high current density of 3200 mA $g^{-1}$), and stable cycling capacity (maintain 800 mAh $g^{-1}$ over long cycles). The excellent electrochemical performance of hierarchical $MoS_2$–C microspheres may be ascribed to their hollow structures which can provide more space for fast mass transport and the bridged carbon between few-layer $MoS_2$ nanosheet which can enhance the electronic conductivity.

Mesoporous $Nb_2O_5$/carbon (m-$Nb_2O_5$-C) nanocomposite has been employed as SIB anode.[29] Besides, ordered mesoporous carbon–$TiO_2$ materials which were synthesized by evaporation-induced self-assembly and *in-situ* crystallization delivered high rate and high cycle durability.[13] The microporous carbide-derived carbon composite (CDC) takes the advantage of the highest specific surface area of more than 3000 $m^2$ $g^{-1}$.[74] It is expected that the electrode materials and high surface carbide-derived carbon composite exhibit high electrochemical performance for supercapacitors. For example, the composite consisting of carbide-derived carbon composite and niobium pentoxide delivered high capacitance after employing this composite as electrode for supercapacitors.[75]

### 3.4. Carbon coated metal oxide composites

Carbon is an abundant element and could be obtained by many adaptable and cheap precursors such as biomass, polymers and glucose. Our group has successfully developed a versatile method to obtain carbon coated materials with high conductivity via polymer assistance chemical solution (PACS) method.[76] For PACS method, water soluble metal salts (e.g metal nitrate, metal chloride and metal hydroxide) bind with a polymer such as *polyethyleneimine* (PEI). The lone electron pairs on the nitrogen atoms of the PEI provide the ability to bind with some metal ions through covalent bonding,

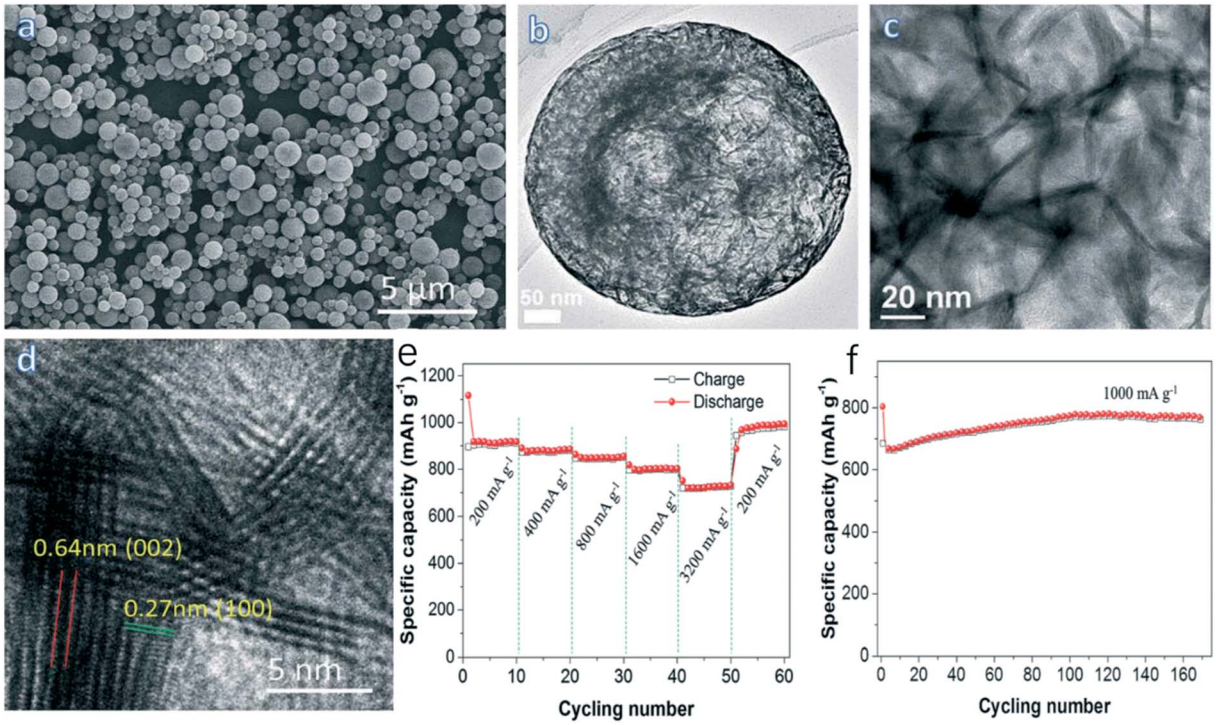


**Fig. 7** SEM image (a), TEM images (b, c) and high resolution TEM image (d) of hierarchical $MoS_2$–C microspheres; (e) rate capacity and cycling performance (f) of the hierarchical $MoS_2$–C microspheres, Adapted and reproduced with the permission from Ref. 73. Copyright 2016, Royal Society of Chemistry.

e.g. Ni and Co.[77,78] Other metal ions (e.g. Mn) that cannot bind to PEI directly could bind to *ethylenediaminetetraacetic acid* (EDTA) to form an EDTA-metal complex via covalent bonding.[16] The binding between the EDTA complexes and PEI could be further strengthened via a combination of hydrogen bonding and electrostatic attraction. Fig. 8 displays the molecular structure of EDTA, PEI, and the bonding with transition metal ions. Foam-like powders of carbon coated metal oxide nanoparticles with high surface area could be achieved after thermal treatment of the metal-polymer complex precursors in furnace under the air. Comparing with other solution methods, PACS owns the unique advantage of preventing the hydrolysis of some metal precursors (e.g niobium chloride and titanium chloride) due to the strong binding between polymers and metal ions.

It is noted that certain amount of carbon coexists with metal oxides when the metal-polymer complex solutions are heated at relatively low temperatures.[79] The carbon generated from the incomplete depolymerization of PEI and EDTA could be *in-situ* coated on the metal oxides. Therefore, the nanoparticle size and the carbon coating thickness can be easily controlled by tuning the heating temperature, time, as well as the concentration of the solutions. The carbon coating also can prevent the agglomeration of metal oxides under heat treatment. More importantly, the carbon coating could enhance the electronic conductivities of pristine metal oxides. Our recent work has showed that two-dimensional $V_2O_5$ sheet network, which was synthesized by a one-step PACS method, was employed as electrode materials for LIBs.[80] From Fig. 9a, a network-like sheet structure could be observed and the thin carbon layer was uniformly coated on the $V_2O_5$ nanoparticles. The thin carbon coating layer remained after the incomplete decomposition of the polymer. The specific network-like sheet structure can enhance charge transfer and lithium ion diffusion speed, resulting in high capacity of about 300 mAh $g^{-1}$ (cathode) and 600 mAh $g^{-1}$ (anode). Carbon coated transition metal oxides (TMOs) nanostructures were firstly proposed to grow on nickel foam by a facile PACS method for binder-free LIB anodes.[79] Fig. 9b presents the growth mechanism of TMOs on nickel foam by PACS method. The polymers can serve as a binder in the growth process. The long polymer chains with strong adsorption of metal ions can tangle on the skeleton of the nickel foam during the synthesis process. The metal ions can be *in-situ* fixed on the skeleton of the nickel foam and further be oxidized to metal oxides under the subsequent annealing process. Fig. 9c displays the SEM images of $Co_3O_4$ nanostructures on the skeleton of nickel foam. We can see from this figure that the nickel foam was uniformly covered by $Co_3O_4$ sheet, which can retain the same shape as the skeleton of nickel foam. The thickness of $Co_3O_4$ sheet is around 100 nm (The cross-section of the $Co_3O_4$ sheet is shown in the inserted picture of Fig. 9c). The $Co_3O_4$ sheets have strong binding with the surface of nickel foam and without any detachment after the strong sonication process. TEM images of Fig. 9d shows that $Co_3O_4$ nanoparticles with diameter of around 30 nm were uniformly coated by thin carbon layers. Similar to carbon coated $V_2O_5$ nanosheet network, the existence of thin carbon layer on the $Co_3O_4$ nanoparticles can serve as binder between $Co_3O_4$ and nickel foam. The interconnected structure and conductive carbon thin layer on $Co_3O_4$ nanoparticles provide a continuous pathway and fast path for lithium ions diffusion and charge transfer during charge and discharge processes. The carbon coated nickel doped $LiMn_2O_4$ cathode has also been synthesized via PACS method. The battery with carbon coated nickel doped $LiMn_2O_4$ cathode exhibited the best durable rate capability, with 100 % of the capacity retained (~100 mAh $g^{-1}$) after 400 cycles at 10 C current rate.[76] The excellent cyclability and rate capability originate from the thin carbon layer formed from incomplete depolymerization of polymers and improved conductivity.[76]

### 3.5. Special structure design of carbon coated metal oxide composites

Carbon coated metal oxide composites can not only increase the electronic conductivity but also stabilize the structure of the electrodes during charge/discharge process. Special structure design (e.g. York shell[81] and peapod-like structure with carbon coating[82,83] of the electrode materials can significantly increase the cycle durability and capacity of batteries. Recent study has reported that MnO nanoparticles confined in carbon shell with peapod-like structure provided 20.6 % void space inside the carbon shell.[82] The carbon shell resulted from self-polymerization of dopamine was uniformly coated on MnO nanowires. The MnO@C core-shell with numerous voids could balance the huge volume change and stabilize the electrode structure, especially under high rate test. However, the

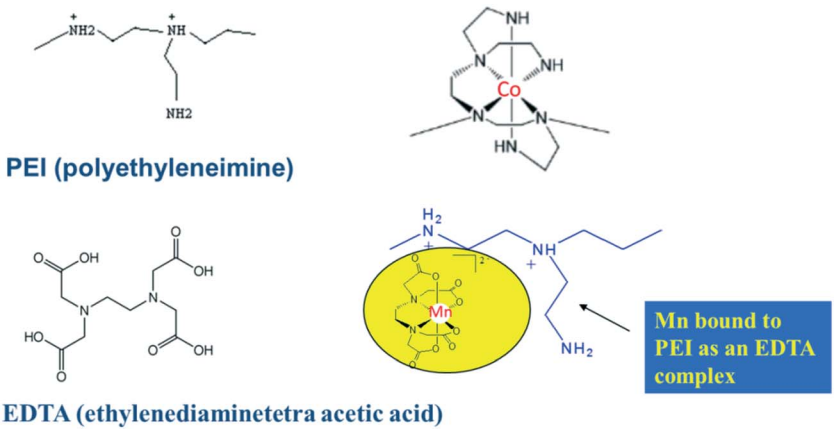


**Fig. 8** The molecular structure of EDTA and PEI, and the bonding with transition metal ions to form metal complexes.

 

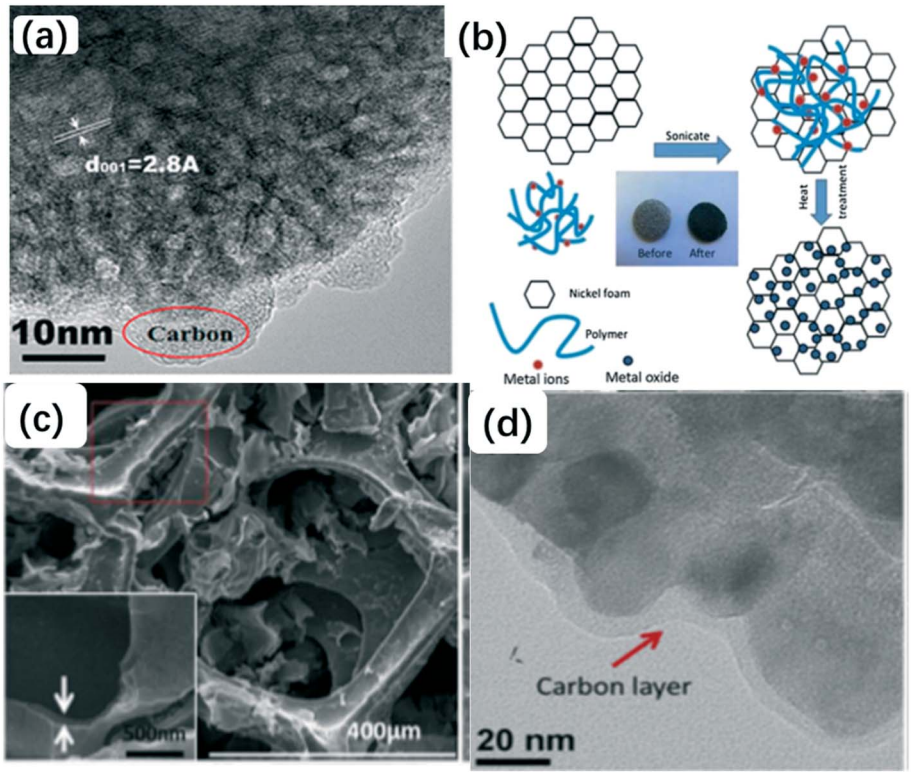


**Fig. 9** HRTEM images of carbon coated $V_2O_5$ (a), schematic mechanism for the growth process of TMOs on nickel foam. The photographs of the original nickel foam (left) and $Co_3O_4$ covered on nickel foam (right) (b); SEM image of $Co_3O_4$ on nickel foam prepared from PACS, the insert is the cross-section of $Co_3O_4$ sheet (c); and TEM image of carbon coated $Co_3O_4$ (d). Adapted and reproduced with the permission from Ref. 80. Copyright 2014, American Chemical Society; Ref. 79, Copyright 2013, Elsevier.

high rate performance of MnO@C core-shell structures is also strongly dependent on the highly conductive carbon shell, which can enhance the electronic conductivity to satisfy the requirement of fast charge transfer under high rate test. Ex-situ TEM (Fig. 10) demonstrated that there is no obvious morphology change after 1000 cycles at high current densities of 2000 mA $g^{-1}$, indicating that MnO@carbon core-shell composites with peapod structure are promising candidate as electrode materials in superior stable energy storage electrochemical devices.[83] Another successful design was to make $Fe_3O_4$@$Fe_3C$ core@shell nanoparticles confined into hollow conductive carbon shell.[81] The specific York-shell structure with sufficient internal void space can introduce more space to maintain the integrity of the electrode structure for high rate and long cycle performance. Moreover, the double shells of both highly conductive $Fe_3C$ and carbon shell not only prevent the dissolution of $Fe_3O_4$, but also increase the conductivity of the active electrode materials. The LIBs with $Fe_3O_4$@$Fe_3C$-C yolk–shell nanospindles as anode materials delivered superior electrochemical performance including high rate capacity and high cycle performance. The void space in carbon shell for huge volume change and contraction as well as the

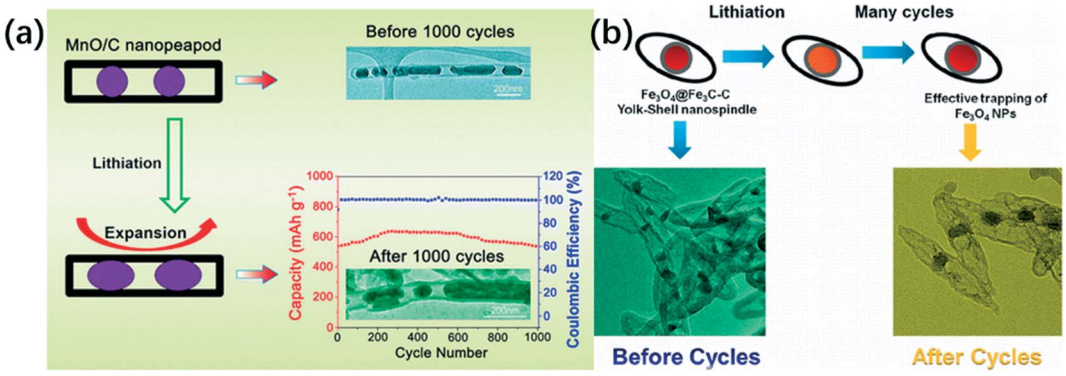


**Fig. 10** The performance of MnO@C core@shell (a) and the cycle durability of $Fe_3O_4$@$Fe_3C$-C yolk–shell nanospindles (b). Adapted and reproduced with the permission from Ref. 81 and Ref. 83. Copyright 2016 and 2014, American Chemical Society.

significant charge transfer enhancement of carbon shell can lead to high electrochemical performance.

### 3.6. Electronic structure modification of electrode materials

Most metal oxides suffer poor electronic conductivity and thereby result in the lower electrochemical performance, especially for titanium or niobium-based oxides with large band gap. Take the intercalation-type $TiNb_xO_{2+2.5x}$ ($x$ = 2, 5 and 24) anode materials as the example, the empty 3d/4d orbitals in $Ti^{4+}/Nb^{5+}$ ions of $TiNb_xO_{2+2.5x}$ lead to their low electronic conductivity (~ $10^{-9}$ S $cm^{-1}$), greatly limiting their practical applications.[84] Various strategies to enhance the conductivities of $TiNb_xO_{2+2.5x}$ have been explored in order to take the advantage of their large theoretical capacities (388–402 mAh $g^{-1}$). In addition to incorporation with conductive carbon-based materials[85–87] or nitridation[88] of surface layer on $TiNb_xO_{2+2.5x}$, modification of the electronic structures via doping other elements and generating oxygen vacancy to improve their conductivities could also be employed. Recently, highly conductive $Cr_{0.5}Nb_{24.5}O_{62}$ (*C2* space group) nanowires with open $ReO_3$ crystal structure have been reported as a class of high performance anode materials for LIBs.[89] The total/partial density of state (DOS) of $Cr_{0.5}Nb_{24.5}O_{62}$ is displayed in Fig. 11a. Fermi level of $Cr_{0.5}Nb_{24.5}O_{62}$ is inside of some band and moves to high energy end, indicating the conductor behavior of $Cr_{0.5}Nb_{24.5}O_{62}$. The 3d orbital of Cr is slightly hybridized with the 2p orbital of oxygen, making the contribution of the bands below the Fermi level. The unpaired 3*d* electrons in the $Cr^{3+}$ ions provide the free transport electron in crystal structure, resulting in $Cr_{0.5}Nb_{24.5}O_{62}$ with high electronic conductive behavior. High electronic conductivity (3.6 × $10^{-2}$ S $cm^{-1}$) of $Cr_{0.5}Nb_{24.5}O_{62}$ nanowire leads to large $Li^+$ ion diffusion coefficient (2.19 × $10^{-13}$ $cm^2$ $s^{-1}$), and thus outstanding electrochemical properties. The reversible capacity of 344 mAh $g^{-1}$ at 0.1 C was the largest capacity among all the reported Nb-based anode materials. Excellent rate capability of 209 mAh $g^{-1}$ at 30 C and superior cycling stability, makes $Cr_{0.5}Nb_{24.5}O_{62}$ high performance anode materials for LIBs with improved safety since high operation potential (> 1.65 V vs $Li/Li^+$) can prevent the formation of lithium dendrites, as shown in Fig. 11b and 11c.

Creating oxygen vacancy is another typical technique to improve the conductivity of metal oxides.[90] The formation of the oxygen vacancy in metal oxides can be described by the Krgoer-Vink equation[91]:

$$2O_O \rightarrow 2V_{\ddot{O}} + 4e^{'}$$

where $O_O$ and $V_{\ddot{O}}$ represent the lattice oxygen and oxygen vacancy, respectively. The formation of oxygen vacancy is also associated with the reduction of valence state of metal based on the defect equation[91,92] (taking vacuum-treated $TiO_2$ as example):

$$2O_O + 4Ti_{Ti} \rightarrow O_2 + 2V_{\ddot{O}} + 4Ti_{Ti}$$

Fig.12a displays the high resolution XPS spectrum of titanium in pristine $TiO_2$ and vacuum treated $TiO_2$ (with generation of oxygen vacancy). A shoulder around 457 eV in vacuum treated $TiO_2$ could be assigned to the characteristic binding energy of $Ti^{3+}$. The partially reduced titanium can provide excessive free electrons in $TiO_2$ crystal structure, leading to highly conductive $TiO_2$. The reversible capacity (140 mAh $g^{-1}$ at 1 C rate) of $TiO_2$ nanocrystals

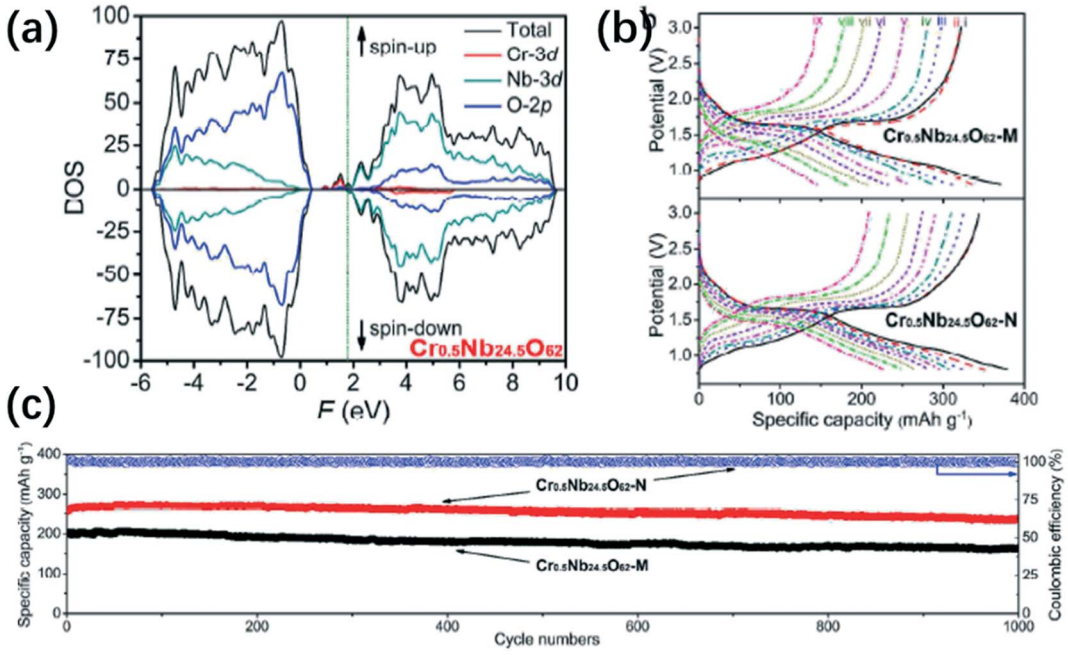


**Fig. 11** (a) Calculated DOS of $Cr_{0.5}Nb_{24.5}O_{62}$; (b) (i) First-cycle discharge–charge curves at 0.1 C and second-cycle discharge–charge curves at different rates of $Cr_{0.5}Nb_{24.5}O_{62}$-M and $Cr_{0.5}Nb_{24.5}O_{62}$-N; and (c) Cycling stability of $Cr_{0.5}Nb_{24.5}O_{62}$ -M and $Cr_{0.5}Nb_{24.5}O_{62}$-N cells at 10 C. Adapted and reproduced with the permission from Ref. 89. Copyright 2017, American Chemical Society.

 

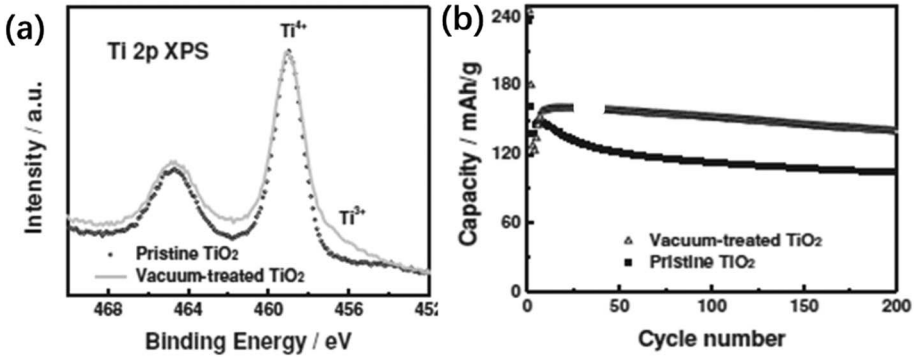


**Fig. 12** XPS spectra of pristine and vacuum-treated $TiO_2$ nanocrystals (a); the capacities of pristine and vacuum-treated $TiO_2$ nanocrystals for the first 200 cycles (b). Adapted and reproduced with the permission from Ref. 93. Copyright 2011, Royal Society of Chemistry.

with oxygen vacancy is 34.6 % higher than that of pristine $TiO_2$ nanocrystals (104 mAh $g^{-1}$), as shown in Fig. 12b.

Oxygen vacancy generation in $TiO_2$ nanotubes has been demonstrated as an effective way to enhance the capacity of titania.[93] The strategy of oxygen vacancy has been also introduced to enhance the performance of SIBs. Recent study has reported that $MoO_{3-x}$ with rich oxygen vacancy can be significantly beneficial to the high electrochemical performance of SIBs[94] since oxygen vacancy can increase the electronic conductivity and ion diffusion coefficient, leading to high reversible capacity and excellent rate capacity as well as high cycle durability. Our group also reported that stoichiometric $Nb_2O_{5-x}$@carbon matrix exhibited high rate and high durability after employing it as anode materials for LIBs (Ref. 84). In our work, the transformation from the stoichiometric $Nb_2O_5$ insulator to $Nb_2O_{5-x}$ semiconductor as well as the uniform distribution of $Nb_2O_{5-x}$ nanocrystals in the carbon matrix can effectively enhance the electronic conductivity and ion diffusion coefficient, leading to the enhanced battery performance by using $Nb_2O_{5-x}$@carbon matrix as electrode material.

### 3.7. Nitridation layer on the pristine electrode materials

Titanium and niobium-based oxides have been developed as promising anode materials for LIBs. Among them, titanium niobium oxide ($TiNb_2O_7$) takes the advantages of high theoretical capacity of 387 mAh $g^{-1}$, high rate performance and improved safety issues

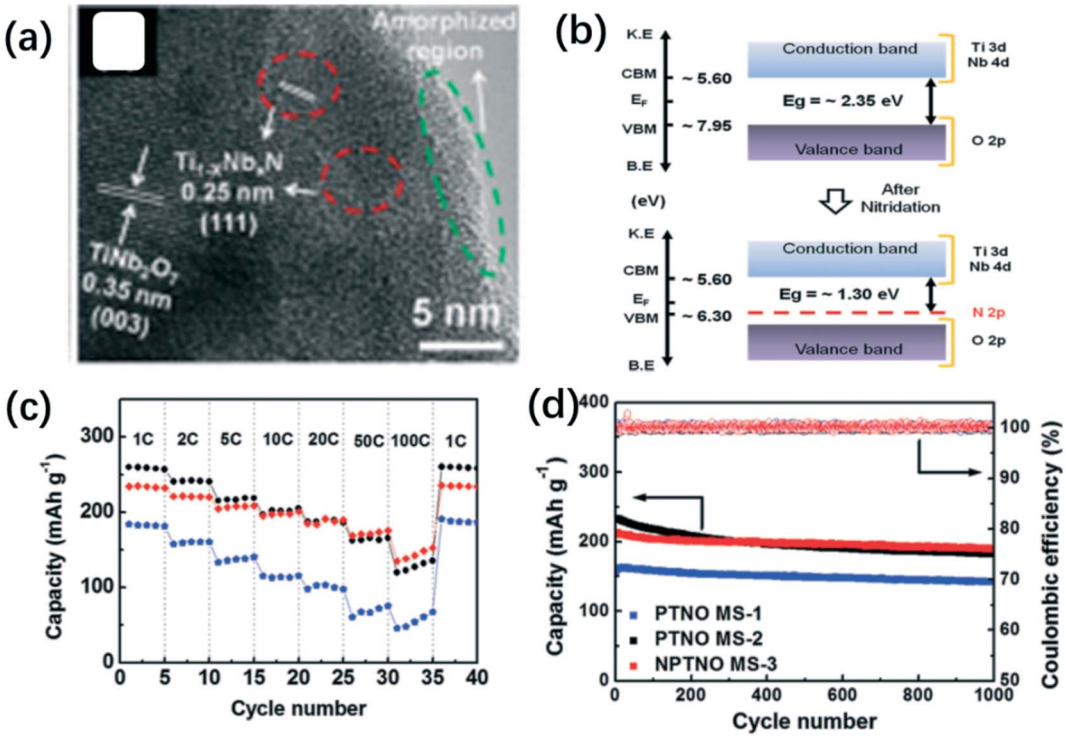


**Fig. 13** (a) High resolution TEM images of nitridation layer on $TiNb_2O_7$; (b) schematic illustration of surface energy band diagram of $TiNb_2O_7$ and nitridation layer on $TiNb_2O_7$; (c) rate capability of $TiNb_2O_7$ and nitridation layer on $TiNb_2O_7$; and (d) cycling performance and their Coulombic efficiencies at 5C. Adapted and reproduced with the permission from Ref. 96. Copyright 2015. WILEY-VCH Verlag GmbH & Co. KGaA, Weinheim.

since the high operation potential can prevent the formation of lithium dendrites.[95] However, the wide band gap energy (> 2 eV) of $TiNb_2O_7$ leads to poor $Li^+$ ion diffusivity and low electronic conductivity which can significantly decrease the battery performance. Recent study has shown that conductive $Ti_{1-x}Nb_xN$ layer on the surface of porous $TiNb_2O_7$ microspheres could be introduced by ammonia gas nitridation heat treatment,[96] as shown in Fig. 13a. The formation of conductive nitridation layer can reduce the band gap of $TiNb_2O_7$ from 2.35 to 1.3 eV (Fig. 13b), leading to the enhancement of the mass and charge transport kinetics associated with $Li^+$ ions (ion diffusion coefficient $\approx 1.4\times10^{-12}$ $cm^2$ $S^{-1}$) and electrons. Consequently, the nitridation layer coated porous $TiNb_2O_7$ microspheres delivered a high discharge capacity of around 265 mAh $g^{-1}$, superior rate capability of about 143 mAh $g^{-1}$ at 100 C and high cycle durability of 91 % capacity retention after 1000 cycles, as shown in Fig. 13c and 13d.

Therefore, nitridation process has been also utilized to increase lithium ion diffusion and electrocatalytic activity of other positive electrode materials for high performance LIBs. For example, one study showed that the nitridated $TiO_2$ hollow fibers delivered two times higher rate capacity compared to pristine $TiO_2$ nanofibers.[97] Besides, nitridation-driven anatase $TiO_2$@graphene composite, $Li_4Ti_5O_{12}$ and $TiO_2$ nanowires have been recognized as anode materials for high performance LIBs.[98] The incorporation of conductive nitridation layer on Li-rich layered $Li[Li_{0.17}Ni_{0.25}Mn_{0.58}]O_2$ oxide results in high rate (164.7 mAh $g^{-1}$ at the current density of 1500 mA $g^{-1}$) and high cycle performance (capacity retention of 256 mAh $g^{-1}$ after 60 cycles).[99] Considering that the easy handling of nitridation process and enhanced conductivity resulted from it, nitridation could be introduced to $TiO_2$/CNTs to further enhance the charge transfer. It is expected that the excellent electronic conductivity of TiON and introducing nitrogen into CNTs could both increase the charge and mass transfer, resulting in the improved capacitance performance.

### 3.8. Electrode materials with dual conductive network

It has been discussed above that electrode materials with surface carbon coating can enhance the conductive behavior and ion diffusion rate. However, the poor electronic conductivity or disconnection between the separated particles still has limited the performance improvement, especially in micro-sized electrode materials. Carbon-based material including mesoporous carbon and graphene with two-dimension structure is usually identified as a conductive media to connect separated particles and thus improve the battery performance by improving charge transfer and maintaining electrical contact in electrodes.[100,101] Thus, it is expected that the active electrode materials sandwiched by dual conductive layers will further enhance the electrode conductivity due to the decrease of the contact resistance of the electrode. Recently, a novel micro-sized graphene@silicon@carbon composite with dual conductive network (Fig. 14a) has been reported as high performance anode materials for LIBs.[102] The electrical resistance of silicon has been significantly decreased by the incorporation of dual conductive network where carbon was coated onto micro-sized silicon and graphene could be used to connect separated micro-size silicon with carbon coating, resulting in better battery performance. Carbon coated $SnO_2$/graphene nanosheet is another example of using dual conductive networks to enhance the

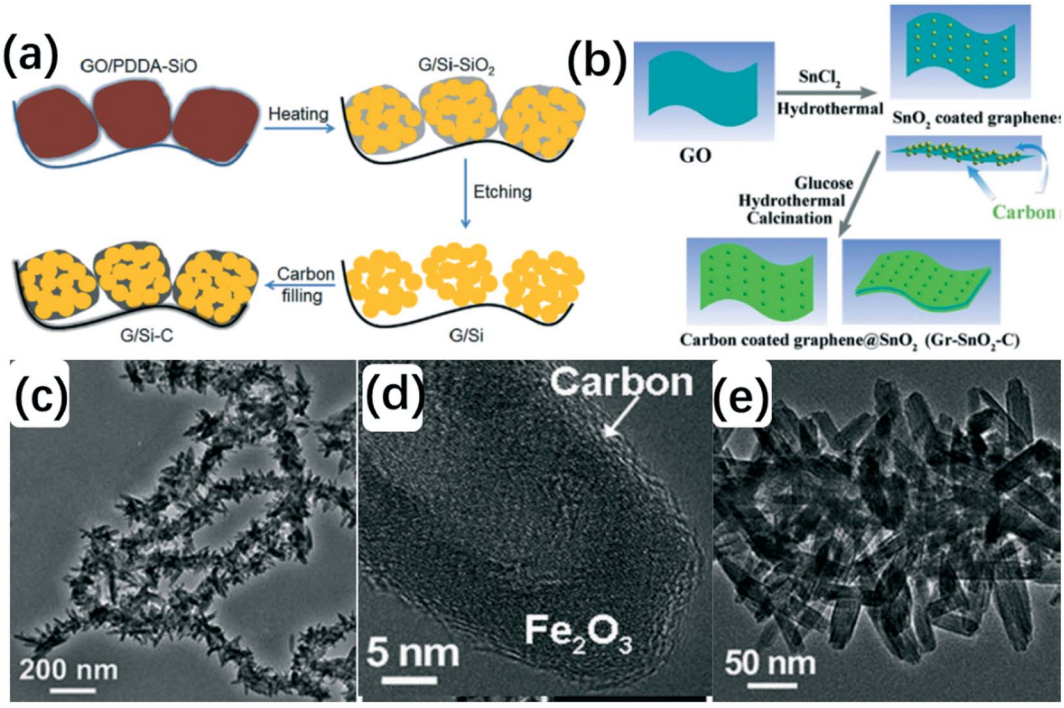


**Fig. 14** Preparation process of G/Si–C. (a); the formation of carbon-coated $SnO_2$/graphene nanosheets (b); and TEM images of carbon@$Fe_2O_3$@CNTs (c-e); Figure a and b is adapted and reproduced with the permission from Ref. 103. Copyright 2014 and Ref. 104, Copyright 2012, Elsevier, respectively; Figure c-d is adapted and reproduced with the permission from Ref. 105. Copyright 2012. Royal Society of Chemistry.

 

electronic conductivity.[103] The illustration of the formation of carbon coated $SnO_2$/graphene nanosheet is displayed in Fig. 14b. The dual conductive network in which $SnO_2$ nanoparticles were wrapped by graphene nanosheets and carbon layer can serve as electron conductor, leading to superior battery performance with large reversible capacity and high cycle durability. Besides, this carbon coated $SnO_2$/graphene nanosheet not only increases the conductivity, but also can maintain the structure and avoid the detachments of $SnO_2$ nanoparticles during cycling. Similar design of 2D core-shell graphene@silicon@carbon has been proposed as the high-performance electrode materials as well.[104] Except for graphene as conductive media, CNTs also serve as the conductive chain to enhance the electronic conductivity. Recently, carbon-coated $Fe_2O_3$ hollow nanohorns uniformly grew on CNTs backbone (carbon@$Fe_2O_3$@CNTs),[105] as shown in Fig. 14c. The combination of highly conductive CNTs backbone and carbon coated layer on $Fe_2O_3$ makes carbon@$Fe_2O_3$@CNTs a durable electrode material for LIBs. Dual conductive network (carbon layer and CNTs or graphene composite) served the same function of conductive matrix in which electrode material is homogenously immersed or distributed into the conductive network. This specific conductive network with superior conductivity can enhance the ion diffusion, charge transfer and maintain the material structure during high rate charge/discharge process.

### 3.9. The incorporation of metal particles or metal coating with electrode materials

Incorporation of metal nanoparticle or coating metal thin layer on electrode is another strategy to increase its conductivity due to the enhanced ion diffusion and the high conductivity of the nanostructured metal architecture. Recently, nanoporous gold/$MnO_2$ thin films with thickness of 100 nm have been successfully prepared by combination of chemical de-alloying and electrodeless plating,[106] as shown in Fig. 15a. The nanoporous gold was prepared by de-alloying Ag65Au35 using $HNO_3$. TEM images (Fig. 15b) showed that the pores were filled with $MnO_2$ nanoparticles. The excellent contact between the gold ligaments and nanocrystalline $MnO_2$ could be confirmed since that $MnO_2$ nanoparticles grew epitaxially on the gold surfaces. The formation of chemically bonded metal/oxide interface caused the manganese L2,3 edges shift to the low-energy side in the gold/$MnO_2$ interface region, resulting in enhanced charge transfer between the gold substrate and $MnO_2$ nanocrystals. The nanoporous gold acts as the good electronic/ionic conductor to enhance the electrochemical performance of $MnO_2$ nanoparticles which are immersed in the nanoporous gold. The nanoporous gold could provide the electron transport path to $MnO_2$ and thus increase ion diffusion rate between the electrolyte and $MnO_2$. The hybrid structure can not only maintain the high specific capacity of $MnO_2$ but also enhance the conductivity of $MnO_2$ (poor conductivity of $10^{-5}$–$10^{-6}$ S $cm^{-1}$), resulting in high specific capacitance of 1145 mAh $g^{-1}$ that is almost close to the theoretical value (1232 mAh $g^{-1}$)[107] of $MnO_2$.

Incorporation of silver nanoparticles on electrode is another typical example to enhance the conductivity. Recent study has found that the electronic conductivity of the Ag/$TiNb_2O_7$ and Ag/ $Li_4Ti_5O_{12}$ (LTO) electrode materials have been significantly increased, leading to fast charge transfer, electron transport and enhancement of electrochemical performance including high cycle and high rate performance.[108, 109] Besides, addition of uniformly dispersed metal in cathode materials has been also demonstrated to increase the conductivity and electrochemical performance. Corce *et al* showed that silver or copper dispersion on phosphor-olivine $LiFeO_4$ did not change the structure of $LiFePO_4$ but decreased the interparticle resistance. LIBs with metal modified $LiFePO_4$ electrodes delivered the enhanced capacity comparing with pristine $LiFePO_4$.[110]

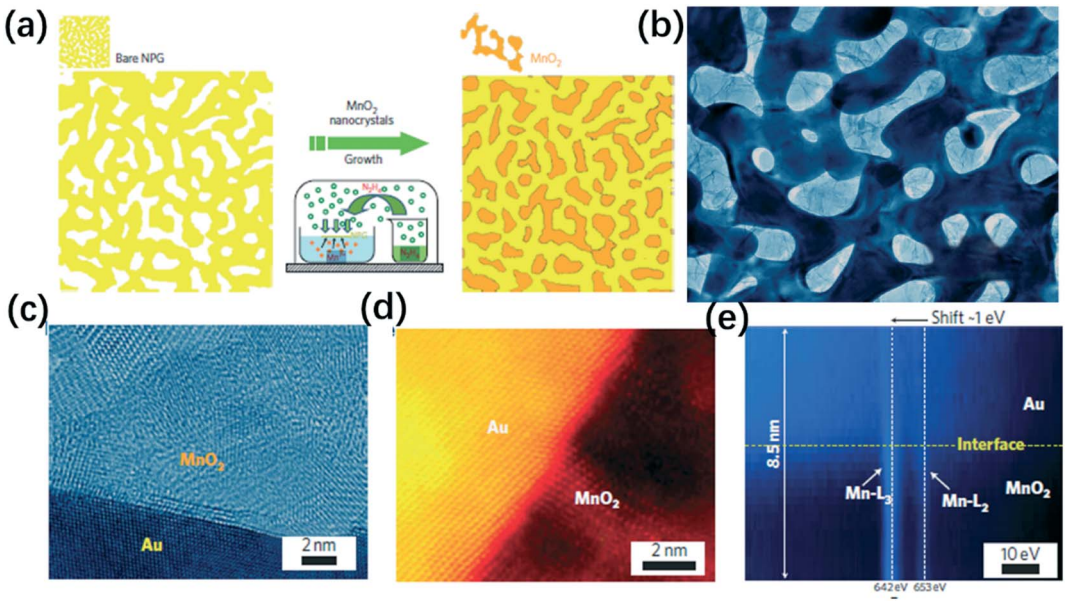


**Fig. 15** The fabrication process for nanoporous gold/$MnO_2$ hybrid materials (a); bright-field TEM image of the nanoporous gold/$MnO_2$ hybrid (b); HRTEM image of nanoporous gold/$MnO_2$ (c); high-angle annular dark-field STEM image taken from the interface between gold/$MnO_2$ (d); and EELS profile image from a region across the interface between gold/$MnO_2$ (e). Adapted and reproduced with the permission from Ref. 106. Copyright 2012. Nature Publish Group.

### 3.10. Conductive polymers on electrode materials

Conductive polymers, such as poly(3,4-ethylenedioxythiophene (PEDOT), due to its excellent conductivity, high stability and mechanical flexibility, could be used as conductive media to improve the charge transfer.[111,112] Recently, it has been reported that 1D rod-like layer manganese oxide could be uniformly distributed on 3D graphene matrix with the assistance of PEDOT. The specific structure with PEDOT coating on $MnO_2$ and 3D graphene matrix provides more surface area for mass transport and enhances the charge transfer to get high rate performance.[111] $MnO_2$/PEDOT coaxial nanowires with 1-D structure have been developed as high performance electrochemical energy storage materials. Highly conductive and porous PEDOT shell increases the mass and charge transfer to core $MnO_2$, leading to that the coaxial nanowires with PEDOT shell coating exhibit high rate performance and excellent cycle durability.[113] Rhombohedral $LiNbO_3$ with poor conductivity is considered to be a promising anode material in LIBs since it owns a large theoretical capacity (363 mAh $g^{-1}$). 3D conductive network consisting of CNTs and conductive polymer polypyrrole (PPy) was introduced to synthesize self-weaving CNT-PPy-$LiNbO_3$ electrodes.[70] The special 3D structure with superior conductivities is composed of $LiNbO_3$ nanoplates, CNTs backbone and PPy coating. This structure can facilitate the mass and charge transfer, yielding larger reversible capacities of around 250 mAh $g^{-1}$ at a current density of 0.4 A $g^{-1}$, an excellent rate capability of 150 mAh $g^{-1}$ at a high rate of 4 A $g^{-1}$ and high cycle durability with a high capacity of 220 mAh $g^{-1}$ which could be maintained after 500 cycles.

## 4. Summary and future perspectives

In this mini review, we have summarized the recent development of highly conductive electrodes for high performance LIBs. Various strategies employed for enhancing the conductivity of the electrode materials have been discussed. Carbon based materials (e.g. graphene, CNTs and porous carbon), which were regarded as the light and high conductive materials, have been the first choice to be utilized to combine with the electrode materials in order to increase their conductivities and subsequently improve the battery performance. Besides, introduction of nitridation layer, conductive polymer layer, oxygen vacancy on electrode materials (usually metal oxides) as well as electrodes being sandwiched by dual conductive networks and so on, could also be utilized as alternatives to improve the conductivities of the electrode materials and subsequently the battery performance.

To make full utilization of carbon-based materials, we have proposed a sol-gel strategy to uniformly coat electrode materials on graphene oxide or functional carbon nanotubes. The strong affinity between metal precursors and functional groups on graphene/reduced graphene oxide or carbon nanotubes can result in the uniform coating. However, the introduction of functional groups could decrease the conductivity and subsequent annealing process under the reduced atmosphere at high temperature is required, which involves complicated and tedious work. Moreover, the synthesis process requires high oxidant reagents and strong acids, leading to some critical environmental issues. It is highlighted that the porous $MoS_2$/C micro-sphere has delivered excellent electrochemical performance including high durability and rate performance. However, considering the sacrifice of volume capacity of battery, the balance between the porous structures of the metal oxides and electrochemical performance should be optimized although the porous structure of electrode materials will be beneficial for ion diffusion. All the aforementioned strategies involve more than two steps, which might introduce extra safety issues and reduce the electrode production efficiency and thus limit the practical applications of LIB/SIBs. Therefore, it would be more convenient to prepare metal oxides on CNTs or graphene as well as other carbon composites using one-step procedure. Moreover, the battery performance with electrode materials growing on nickel foam by PACS method has demonstrated that PACS will be an effective method to prepare electrode materials on substrate or support directly. Therefore, the future work of our group will focus on uniformly coating electrode on carbon-based materials by a versatile PACS method, through which highly conductive electrode materials could be prepared via one-step reaction.

## Acknowledgements

Dr. Luo thanks the support from New Mexico EPSCoR with NSF-1301346 and USDA National Institute of Food and Agriculture, HSI Collaboration: Integrating Food Science/Engineering and Education Network (IFSEEN, award number: 2015-38422-24059).

## References

1 L. Yan, J. Yu, J. Houston, N. Flores and H. Luo, *Green Energy & Environ.*, 2017, **2**, 84–89.
2 F. Cheng and J. Chen, *Chem. Soc. Rev.*, 2012, **41**, 2172–2192.
3 X. Zhang, H. Zhang, C. Li, K. Wang, X. Sun and Y. Ma, *RSC Adv.*, 2014, **4**, 45862–45884.
4 X. H. Rui, Q. Y. Yan, M. Skyllas-Kazacos and T. M. Lim, *J. Power Sources*, 2014, **258**, 19–38.
5 X. Rui, H. Tan and Q. Yan, *Nanoscale*, 2014, **6**, 9889–9924.
6 D. Aurbach, *J. Power Sources*, 2003, **119–121**, 497–503.
7 X. Zheng and J. Li, *Ionics*, 2014, **20**, 1651–1663.
8 X. Su, Q. Wu, X. Zhan, J. Wu, S. Wei and Z. Guo, *J. Mater. Science*, 2012, **47**, 2519–2534.
9 R. Yi, M. L. Gordin and D. Wang, *Nanoscale*, 2016, **8**, 1834–1848.
10 L. Zhao, Y.-S. Hu, H. Li, Z. Wang and L. Chen, *Adv. Mater.*, 2011, **23**, 1385–1388.
11 H. Jin, Z. Cui, W. Zhou, L. Guo and S. Yang, *Sci. China-Technol. Sci.*, 2012, **56**, 8–12.
12 J.-Y. Shin, J. H. Joo, D. Samuelis and J. Maier, *Chem. Mater.*, 2012, **24**, 543–551.
13 P.-y. Chang, C.-h. Huang and R.-a. Doong, *Carbon*, 2012, **50**, 4259–4268.
14 L. Fei, Q. Lin, B. Yuan, G. Chen, P. Xie, Y. Li, Y. Xu, S. Deng, S. Smirnov and H. Luo, *ACS Appl. Mater. Inter.*, 2013, **5**, 5330–5335.
15 Z. Bi, M. P. Paranthaman, P. A. Menchhofer, R. R. Dehoff, C. A. Bridges, M. Chi, B. Guo, X.-G. Sun and S. Dai, *J. Power Sources*, 2013, **222**, 461–466.
16 Y. Jiang, G. Chen, X. Xu, X. Chen, S. Deng, S. Smirnov, H. Luo and G. Zou, *RSC Adv.*, 2014, **4**, 48938–48942.

 

17 G. Chen, R. Rodriguez, L. Fei, Y. Xu, S. Deng, S. Smirnov and H. Luo, *J. Power Sources*, 2014, **259**, 227–232.
18 G. Chen, M. Zhou, J. Catanach, T. Liaw, L. Fei, S. Deng and H. Luo, *Nano Energy*, 2014, **8**, 126–132.
19 T. Yang, Y. Liu, Z. Huang, Q. Yang, Y. Chen, M. Hu, M. Guan and M. Fang, *RSC Adv.*, 2014, **4**, 41578–41583.
20 H. Li, R. Xu, Y. Wang, B. Qian, H. Wang, L. Chen, H. Jiang, Y. Yang and Y. Xu, *RSC Adv.*, 2014, **4**, 51960–51965.
21 L. Hu, Y. Ren, H. Yang and Q. Xu, *ACS Appl. Mater. Inter.*, 2014, **6**, 14644–14652.
22 T. Ohzuku and Y. Makimura, *Chem. Lett*, 2001, **30**, 642–643.
23 J.-C. Li, Z. Ma, Y. Chi and S.-P. Guo, *J. Mater. Sci.*, 2016, 1–8.
24 A. S. Hameed, M. V. Reddy, J. L. T. Chen, B. V. R. Chowdari and J. J. Vittal, *ACS Sustain. Chem. Eng.*, 2016, **4**, 2479–2486.
25 Z.-G. Wu, J.-T. Li, Y.-J. Zhong, J. Liu, K. Wang, X.-D. Guo, L. Huang, B.-H. Zhong and S.-G. Sun, *J. Alloy. Compd.*, 2016, **688, Part B**, 790–797.
26 L. Pan, Y. Liu, X. Xie, X. Ye and X. Zhu, *Nano Res.*, 2016, **9**, 2057–2069.
27 D. Wang, D. Choi, J. Li, Z. Yang, Z. Nie, R. Kou, D. Hu, C. Wang, L. V. Saraf, J. Zhang, I. A. Aksay and J. Liu, *ACS Nano*, 2009, **3**, 907–914.
28 M. Lengyel, G. Atlas, D. Elhassid, P. Y. Luo, X. Zhang, I. Belharouak and R. L. Axelbaum, *J. Power Sources*, 2014, **262**, 286–296.
29 E. Lim, H. Kim, C. Jo, J. Chun, K. Ku, S. Kim, H. I. Lee, I.-S. Nam, S. Yoon, K. Kang and J. Lee, *ACS Nano*, 2014, **8**, 8968–8978.
30 Y.-L. Tang, F. Hou and Y. Zhou, *Mater. Technol.*, 2016, **7**, 377–383.
31 C. Hu, S. Guo, G. Lu, Y. Fu, J. Liu, H. Wei, X. Yan, Y. Wang and Z. Guo, *Electrochim. Acta*, 2014, **148**, 118–126.
32 G. Wang, S. Zhou, H. Wang, Z. Ren and J. Bai, *Science of Adv. Mater.*, 2015, **7**, 1272–1281.
33 A. S. Arico, P. Bruce, B. Scrosati, J. M. Tarascon and W. Van Schalkwijk, *Nat. Mater*, 2005, **4**, 366–377.
34 F. Y. Cheng, J. Liang, Z. L. Tao and J. Chen, *Adv. Mater.*, 2011, **23**, 1695–1715.
35 Y. Xiong, J. Qian, Y. Cao, X. Ai and H. Yang, *J. Mater. Chem. A*, 2016, **4**, 11351–11356.
36 M. R. Arcila-Velez, J. Zhu, A. Childress, M. Karakaya, R. Podila, A. M. Rao and M. E. Roberts, *Nano Energy*, 2014, **8**, 9–16.
37 J. Chen, J. Xu, S. Zhou, N. Zhao and C.-P. Wong, *Nano Energy*, 2015, **15**, 719–728.
38 J. P. Zheng, P. J. Cygan and T. R. Jow, *J. Electrochem. Soc.*, 1995, **142**, 2699–2703.
39 M. Sawicki and L. L. Shaw, *RSC Adv.*, 2015, **5**, 53129–53154.
40 P. Roy and S. K. Srivastava, *J. Mater. Chem. A*, 2015, **3**, 2454–2484.
41 S. Bose, T. Kuila, A. K. Mishra, R. Rajasekar, N. H. Kim and J. H. Lee, *J. Mater. Chem.*, 2012, **22**, 767–784.
42 Y. Wang, Y. Huang, Q. Wang and M. Zong, *Powder Technol.*, 2013, **249**, 304–308.
43 C. Yang, L. Dong, Z. Chen and H. Lu, *J. Phys. Chem. C*, 2014, **118**, 18884–18891.
44 J. L. Zhang, H. D. Liu, L. H. Huang, S. Z. Tan, W. J. Mai and X. Cai, *J. Solid State Electrochem.*, 2014, **19**, 229–239.
45 S. Kong, Z. Jin, H. Liu and Y. Wang, *J. Phys. Chem. C*, 2014, **118**, 25355–25364.
46 M. Wang, J. Huang, M. Wang, D. Zhang and J. Chen, *Food Chem.*, 2014, **151**, 191–197.
47 J. X. Zhu, T. Zhu, X. Z. Zhou, Y. Y. Zhang, X. W. Lou, X. D. Xiao, H. Zhang, H. H. Hng and Q. Y. Yan, *Nanoscale*, 2011, **3**, 1084–1089.
48 H. Liu, Z. Hu, Y. Su, H. Ruan, R. Hu and L. Zhang, *Appl. Surf. Sci.*, 2017, **392**, 777–784.
49 P. Zhao, H. Cui, J. Luan, Z. Guo, Y. Zhou and H. Xue, *Materials Letters*, 2017, **186**, 62–65.
50 J. Shen, Y. Zhu, H. Jiang and C. Li, *Nano Today*, 2016, **11**, 483–520.
51 J. He, P. Li, W. Lv, K. Wen, Y. Chen, W. Zhang, Y. Li, W. Qin and W. He, *Electrochim. Acta*, 2016, **215**, 12–18.
52 B. Zhao, Z. Wang, Y. Gao, L. Chen, M. Lu, Z. Jiao, Y. Jiang, Y. Ding and L. Cheng, *Appl. Surf. Sci.*, 2016, **390**, 209–215.
53 P. Liu, Y. Huang and X. Zhang, *Materials Letters*, 2014, **136**, 298–301.
54 J. Zhou, J. Li, K. Liu, L. Lan, H. Song and X. Chen, *J. Mater. Chem. A*, 2014, **2**, 20706–20713.
55 Y. Park, M. Oh, J. S. Park, S.-H. Baek, M. Kim, S. Kim and J. H. Kim, *Carbon*, 2015, **94**, 9–17.
56 Y. Ma, H. D. Asfaw and K. Edström, *Chem. Mater.*, 2015, **27**, 3957–3965.
57 L. Kong, C. Zhang, J. Wang, W. Qiao, L. Ling and D. Long, *ACS Nano*, 2015, **9**, 11200–11208.
58 L. Fei, B. P. Williams, S. H. Yoo, J. M. Carlin and Y. L. Joo, *Chem. Commu.*, 2016, **52**, 1501–1504.
59 Z. Yang, D. Choi, S. Kerisit, K. M. Rosso, D. Wang, J. Zhang, G. Graff and J. Liu, *J. Power Sources*, 2009, **192**, 588–598.
60 L. T. Yan, J. L. Yu and H. M. Luo, *Applied Materials Today*, 2017, **8**, 31–34.
61 L. Yan, G. Chen, S. Sarker, S. Richins, H. Wang, W. Xu, X. Rui and H. Luo, *ACS Appl. Mater. Inter.*, 2016, **8**, 22213–22219.
62 L. Fei, Q. Lin, B. Yuan, M. Naeemi, Y. Xu, Y. Li, S. Deng and H. Luo, *Mater. Lett.*, 2013, **98**, 59–62.
63 Q. Qu, J. Chen, X. Li, T. Gao, J. Shao and H. Zheng, *J. Mater. Chem. A*, 2015, **3**, 18289–18295.
64 C. F. Lin, L. Hu, C. B. Cheng, K. Sun, X. K. Guo, Q. Shao, J. B. Li, N. Wang and Z. H. Guo, *Electrochim. Acta*, 2018, **260**, 65–72.
65 L. Hu, R. H. Lu, L. F. Tang, R. Xia, C. F. Lin, Z. B. Luo, Y. J. Chen and J. B. Li, *J. Alloy. Compd.*, 2018, **732**, 116–123.
66 C. F. Lin, X. Y. Fan, Y. L. Xin, F. Q. Cheng, M. O. Lai, H. H. Zhou and L. Lu, *J. Mater. Chem. A*, 2014, **2**, 9982–9983.
67 C. F. Lin, B. Ding, Y. L. Xin, C. F. Q, M. O. Lai, L. Lu and H. H. Zhou, *J. Power Sources*, 2014, **248**, 1034–1041.
68 H. Xia, M. Lai and L. Lu, *J. Mater. Chem.*, 2010, **20**, 6896–6902.
69 Y. Wu, Y. Wei, J. Wang, K. Jiang and S. Fan, *Nano Letters*, 2013, **13**, 818–823.
70 Q. Fan, L. Lei, G. Yin and Y. Sun, *Chem. Commu.*, 2014, **50**, 2370–2373.
71 L. Yan, Y. Xu, M. Zhou, G. Chen, S. Deng, S. Smirnov, H. Luo and G. Zou, *Electrochim. Acta*, 2015, **169**, 73–81.
72 L. Fei, Y. Xu, X. Wu, G. Chen, Y. Li, B. Li, S. Deng, S.

Smirnov, H. Fan and H. Luo, *Nanoscale*, 2014, **6**, 3664–3669.
73 G. Chen, S. Wang, R. Yi, L. Tan, H. Li, M. Zhou, L. Yan, Y. Jiang, S. Tan, D. Wang, S. Deng, X. Meng and H. Luo, *J. Mater. Chem. A*, 2016, **4**, 9653–9660.
74 M. Rose, E. Kockrick, I. Senkovska and S. Kaskel, *Carbon*, 2010, **48**, 403–407.
75 C. Zhang, R. Maloney, M. R. Lukatskaya, M. Beidaghi, B. Dyatkin, E. Perre, D. Long, W. Qiao, B. Dunn and Y. Gogotsi, *J. Power Sources*, 2015, **274**, 121–129.
76 Y. Xu, G. Chen, E. Fu, M. Zhou, M. Dunwell, L. Fei, S. Deng, P. Andersen, Y. Wang, Q. Jia and H. Luo, *RSC Adv.*, 2013, **3**, 18441–18445.
77 A. K. Burrell, T. Mark McCleskey and Q. X. Jia, *Chem. Commu.*, 2008, 1271–1277.
78 G. F. Zou, J. Zhao, H. M. Luo, T. M. McCleskey, A. K. Burrell and Q. X. Jia, *Chem. Soc. Rev.*, 2013, **42**, 439–449.
79 Y. Xu, L. Fei, E. Fu, B. Yuan, J. Hill, Y. Chen, S. Deng, P. Andersen, Y. Wang and H. Luo, *J. Power Sources*, 2013, **242**, 604–609.
80 Y. Xu, M. Dunwell, L. Fei, E. Fu, Q. Lin, B. Patterson, B. Yuan, S. Deng, P. Andersen, H. Luo and G. Zou, *ACS Appl. Mater. Inter.*, 2014, **6**, 20408–20413.
81 J. Zhang, K. Wang, Q. Xu, Y. Zhou, F. Cheng and S. Guo, *ACS Nano*, 2015, **9**, 3369–3376.
82 S. Wang, Y. Xing, C. Xiao, H. Xu and S. Zhang, *J. Power Sources*, 2016, **307**, 11–16.
83 H. Jiang, Y. Hu, S. Guo, C. Yan, P. S. Lee and C. Li, *ACS Nano*, 2014, **8**, 6038–6046.
84 Q. Cheng, J. Liang, N. Lin, C. Guo, Y. Zhu and Y. Qian, *Electrochim. Acta*, 2015, **176**, 456–462.
85 A. G. Ashish, P. Arunkumar, B. Babu, P. Manikandan, S. Sarang and M. M. Shaijumon, *Electrochim. Acta*, 2015, **176**, 285–292.
86 S. Li, X. Cao, C. N. Schmidt, Q. Xu, E. Uchaker, Y. Pei and G. Z. Cao, *J. Mater. Chem. A*, 2016, **4**, 4242–4251.
87 G. Z. Zhu, Q. Li, Y. H. Zhao and R. C. Che, *ACS Appl. Mater. Inter.*, 2017, **9**, 41258–41264.
88 H. Park, H. B. Wu, T. Song, X. W. Lou and U. Paik, *Adv. Energy Mater.*, 2015, 1401945.
89 C. Yang, S. Yu, C. Lin, F. Lv, S. Wu, Y. Yang, W. Wang, Z.-Z. Zhu, J. Li, N. Wang and S. Guo, *ACS Nano*, 2017, **11**, 4217–4224.
90 T. Xia, W. Zhang, J. B. Murowchick, G. Liu and X. Chen, *Adv. Energy Mater.*, 2013, **3**, 1516–1523.
91 F. A. Kröger and H. J. Vink, *Solid State Phys.*, 1956, **3**, 307–435.
92 P. A. Burr and M. W. D. Cooper, *Phys. Rev. B*, 2017, **96**, 094107.
93 M. Salari, K. Konstantinov and H. K. Liu, *J. Mater. Chem.*, 2011, **21**, 5128–5133.
94 Y. Xu, M. Zhou, X. Wang, C. Wang, L. Liang, F. Grote, M. Wu, Y. Mi and Y. Lei, *Angew. Chem. Int. Ed. Engl.*, 2015, **54**, 8768–8771.
95 H. Li, L. Shen, G. Pang, S. Fang, H. Luo, K. Yang and X. Zhang, *Nanoscale*, 2015, **7**, 619–624.
96 H. Park, H. B. Wu, T. Song, X. W. Lou and U. Paik, *Adv. Energy Mater.*, 2015, **5**, 1401945.
97 H. Han, T. Song, J.-Y. Bae, L. F. Nazar, H. Kim and U. Paik, *Energ. Environ. Sci.*, 2011, **4**, 4532–4536.
98 Y. Qiu, K. Yan, S. Yang, L. Jin, H. Deng and W. Li, *ACS Nano*, 2010, **4**, 6515–6526.
99 H. Z. Zhang, Q. Q. Qiao, G. R. Li, S. H. Ye and X. P. Gao, *J. Mater. Chem.*, 2012, **22**, 13104–13109.
100 H.-C. Tao, X.-L. Yang, L.-L. Zhang and S.-B. Ni, *J. Electroanal. Chem.*, 2014, **728**, 134–139.
101 H.-C. Tao, X.-L. Yang, L.-L. Zhang and S.-B. Ni, *J. Phys. Chem. Solids*, 2014, **75**, 1205–1209.
102 R. Yi, J. Zai, F. Dai, M. L. Gordin and D. Wang, *Nano Energy*, 2014, **6**, 211–218.
103 C. Zhang, X. Peng, Z. Guo, C. Cai, Z. Chen, D. Wexler, S. Li and H. Liu, *Carbon*, 2012, **50**, 1897–1903.
104 B. Wang, X. Li, X. Zhang, B. Luo, M. Jin, M. Liang, S. A. Dayeh, S. T. Picraux and L. Zhi, *ACS Nano*, 2013, **7**, 1437–1445.
105 Z. Wang, D. Luan, S. Madhavi, Y. Hu and X. W. Lou, *Energ. Environ. Sci.*, 2012, **5**, 5252–5256.
106 X. Lang, A. Hirata, T. Fujita and M. Chen, *Nat. Nano*, 2011, **6**, 232–236.
107 L. L. Feng, Z. W. Xuan, H. B. Zhao, Y. Bai, J. M. Guo, C. W. Su and X. K. Chen, *Nanoscal. Res. Lett.*, 2014, **9**, 290–296.
108 S. H. Nam, H.-S. Shim, Y.-S. Kim, M. A. Dar, J. G. Kim and W. B. Kim, *ACS Appl. Mater. Inter.*, 2010, **2**, 2046–2052.
109 G. Liu, X. Liu, Y. Zhao, X. Ji and J. Guo, *Mater. Lett.*, 2017, **197**, 38–40.
110 F. Croce, A. D' Epifanio, J. Hassoun, A. Deptula, T. Olczac and B. Scrosati, *Electrochem. Solid-State Lett.*, 2002, **5**, A47–A50.
111 C. X. Guo, M. Wang, T. Chen, X. W. Lou and C. M. Li, *Adv. Energy. Mater.*, 2011, **1**, 736–741.
112 L. Cui, J. Gao, T. Xu, Y. Zhao and L. Qu, *Chem-Asian J.*, 2016, **11**, 1151–1168.
113 R. Liu and S. B. Lee, *J. Am. Chem. Soc.*, 2008, **130**, 2942–2943.

 